Urinary Clusterin is a biomarker of renal epithelial senescence and predicts human kidney disease progression

David Baird[1*°], Maximillian Reck[1°], Ross Campbell[1], Marie-Helena Docherty[1], Matthieu Vermeren[1], Andy Nam[3], Wei Yang[3], Nathan Schurman[3], Claire Williams[3], Jamie P. Traynor[2], Patrick B. Mark[2], Katie Mylonas[1], Jeremy Hughes[1], Laura Denby[1], Bryan Conway[1°], David A Ferenbach[1°]

[1]University of Edinburgh, UK. [2]University of Glasgow, UK. [3]Nanostring, Seattle, WA.

[*]Corresponding author. [°]Contributed equally.

Abstract

Cellular senescence drives organ fibrosis and ageing, and accumulating evidence supports the ability of senescence-depleting drugs to improve outcomes in experimental models of disease. The lack of non-invasive biomarkers represents a major obstacle to the design of human trials of candidate senolytics. On samples from 51 patients with chronic kidney disease (CKD), we performed liquid chromatography mass spectrometry (LC-MS) analysis of urine samples alongside immunofluorescence staining of paired kidney biopsies for p21, Ki67, and CD10+Pancytokeratin as senescence, proliferation and pan-epithelial cell markers respectively. Only Urinary Clusterin (uClusterin) correlated tightly with p21+ epithelial senescence *in vivo* (rho >0.5, p<0.001) and was upregulated in the *in vitro* SASP atlas. This was validated in a second cohort of matched urine and kidney samples from n=53 participants, with uClusterin predicting levels of senescence after adjusting for renal function, age and albuminuria. In spatial transcriptomic data from n=13 CKD patients, Clusterin colocalised with senescence marker CDKN1A. In a larger cohort of n=322 participants, elevated levels of uClusterin predicted CKD progression (defined as reaching ESKD or >40% reduction in renal function) after adjusting for baseline eGFR, albuminuria, age, systolic blood pressure (SBP) and sex. uClusterin levels represents a surrogate for histological quantification of p21+Ki67- senescent renal epithelia and predicts outcomes in human kidney disease independent of existing clinical risk factors.

Cellular senescence drives organ fibrosis and ageing, and accumulating evidence supports the ability of senescence-depleting drugs ('senolytics') to improve outcomes in experimental models of disease(1). With no non-invasive biomarkers available, quantifying senescence in human solid organs requires tissue biopsy to identify cells expressing cyclin dependent kinase inhibitors p21 and/or $p16^{INK4A}$ in the absence of proliferation markers. This represents a major obstacle to the design of human trials of candidate senolytics and assessment of treatment responses.

In human chronic kidney disease (CKD), a condition affecting over 850 million people worldwide, p21 protein expression is upregulated in sub-populations of renal epithelia. Levels of *CDKN1A* (encoding p21) transcript correlate with worsened kidney function, (2). The Kidney Precision Medicine Project dataset demonstrated upregulated *CDKN1A* (p21) expression in 'late-adaptive' proximal tubular (PT) epithelia in human CKD (3). *In vitro,* irradiated, Ki67 negative human PT cells expressing p21 upregulated multiple senescence-associated transcripts (2). *In vivo*, our recent multi-omic atlas of human kidney disease confirmed that CDKN1A (p21) expression was upregulated in a proximal tubular subset expressing key DEGs of KPMP 'late-adaptive' PTs' alongside multiple senescence-associated DEGs(4).

We addressed the hypothesis that senescent renal epithelia could be quantified non-invasively by detecting their selectively secreted proteins in human urine samples.

To identify urinary proteins correlating with tubular cell senescence, we first performed high-performance liquid chromatography with tandem mass spectrometry (LC-MS) analysis of 51 urine samples from the Non-invasive biomarkers of renal disease (seNSOR) CKD biobank ('discovery' cohort, Fig A, Fig S1A, Supplemental materials and methods, Table S1A), alongside staining of paired kidney biopsies for p21, Ki67, and CD10+Pancytokeratin as senescence, proliferation and pan-epithelial cell markers respectively (Fig B, Fig S1B). 331 distinct proteins were detected by LC-MS (Table S2), of which 81 had a positive correlation with proportion of $p21^{+}Ki67^{-}$ senescent epithelia (adj $p<0.05$) with 8 having a correlation coefficient (rho)>0.5 (Fig C). Results were compared

to proteins upregulated in the 'SASP atlas' of senescent human renal epithelia *in vitro (5)*. Urinary Clusterin (uClusterin) alone correlated tightly with p21+ epithelial senescence *in vivo* (Fig C, rho >0.53, p<0.001) and was upregulated in the *in vitro* SASP atlas (5). $p21^{+}Ki67^{-}$ senescent epithelial proportions also correlated with increasing patient age and urinary albumin:creatinine ratio (uACR) and inversely with estimated glomerular filtration rate (eGFR) (Fig S1C-E). uClusterin was quantified using ELISA in this discovery cohort and corrected for urinary concentration against urinary creatinine (Fig S1F). Multivariate analysis demonstrated that uClusterin:Creatinine levels predicted p21+Ki67- senescent renal epithelia levels after correction for eGFR, Age and uACR (Fig D).

Studies have shown increased Clusterin secretion from human cells undergoing senescence *in vivo* in other organs (6). To determine whether Clusterin production was selectively increased in $p21^{+}Ki67^{-}$ senescent renal epithelia, sub-cellular resolution spatial transcriptomic analysis (Nanostring CosMx) was performed on kidney tissue from 13 patients with CKD. CLU transcript levels were increased within CDKN1A expressing proximal tubular epithelia on automated counting and co-localisation analysis (n=114,135 epithelia, pAdj=3.91×10^{-8}, Figs E & F).

Given the spatial transcript co-localisation between CLU and CDKN1A and the correlation between urinary Clusterin and histological evidence of p21+ growth arrest, we confirmed our findings in a validation cohort of CKD patients from Glasgow (Fig A, Table S1A). Urinary Clusterin:creatinine ratio again correlated strongly with $p21^{+}Ki67^{-}$ senescent epithelial cell proportions (rho=0.61, p<0.001, Fig S1G), with adjusted uClusterin:creatinine levels predicting histological senescence after correction for eGFR, uACR and Age (Fig D).

Next, we explored the optimal uClusterin:Creatinine ratio required to identify patients with high levels of $p21^{+}Ki67^{-}$ senescent epithelia. By prioritising high specificity over high sensitivity, a threshold of 124.5 µg Clusterin/mmol Creatinine was selected. This corresponded to a sensitivity of 68% and specificity of 90% for identifying those with the

highest tertile of $p21^{+}Ki67^{-}$ senescent epithelia, with the AUC of the receiver operating characteristic (ROC) 81.2% (Fig S1H).

We tested whether the uClusterin:Creatinine ratio predicted a decline in renal function in 322 patients with CKD (Fig G, Fig S1A). The composite CKD progression endpoint (defined as reaching ESKD or >40% reduction in renal function from eGFR at baseline) occurred in 47 (15%) participants during 3 years follow-up.

76 participants had uClusterin:Creatinine levels >124.5 µg/mmol. These participants had a higher risk of CKD progression (log-rank $p < 0.001$, Fig H). In Cox Proportional Hazards analysis, a uClusterin:Creatinine level above 124.5 µg/mmol predicted CKD progression after adjusting for baseline eGFR, uACR, age, systolic blood pressure (SBP) and sex in multivariate analysis (HR 2.2, 95% C.I. 1.07-4.66, p=0.03, Fig I). Including uClusterin:Creatinine levels as continuous variables (either untransformed or log-transformed) in models was also significant and additive to biomarkers currently used in clinical practice for predicting CKD progression in multivariate analyses (Table S3).

This study demonstrates that measurement of uClusterin:Creatinine levels represents a surrogate for histological quantification of $p21^{+}Ki67^{-}$ senescent renal epithelia and predicts outcomes in human kidney disease independent of and additively to existing clinical risk factors. These findings provide additional evidence connecting human renal epithelial senescence to functional decline in kidney disease. They also demonstrate the ability of non-invasive biomarkers to quantify senescent cells in solid organs and identify patients at elevated risk of progressive kidney disease for trial recruitment and targeting of senolytic therapies and monitoring of therapeutic response.

REFERENCES

1. Dolgin E. Send in the senolytics. Nature biotechnology. 2020;38(12):1371-7.
2. Mylonas KJ, et al. Cellular senescence inhibits renal regeneration after injury in mice, with senolytic treatment promoting repair. Science translational medicine. 2021;13(594).
3. Lake BB, et al. An atlas of healthy and injured cell states and niches in the human kidney. Nature. 2023;619(7970):585-94.
4. Conway B, et al. Multiomic analysis of human kidney disease identifies a tractable inflammatory, pro-fibrotic tubular cell phenotype. 2024.
5. Basisty N, et al. A proteomic atlas of senescence-associated secretomes for aging biomarker development. PLoS biology. 2020;18(1):e3000599.
6. Antonelou MH, et al. Apolipoprotein J/Clusterin is a novel structural component of human erythrocytes and a biomarker of cellular stress and senescence. PLoS One. 2011;6(10):e26032.

Figure Legend: Discovery and validation of urinary Clusterin as a biomarker of renal senescence and patient outcomes.

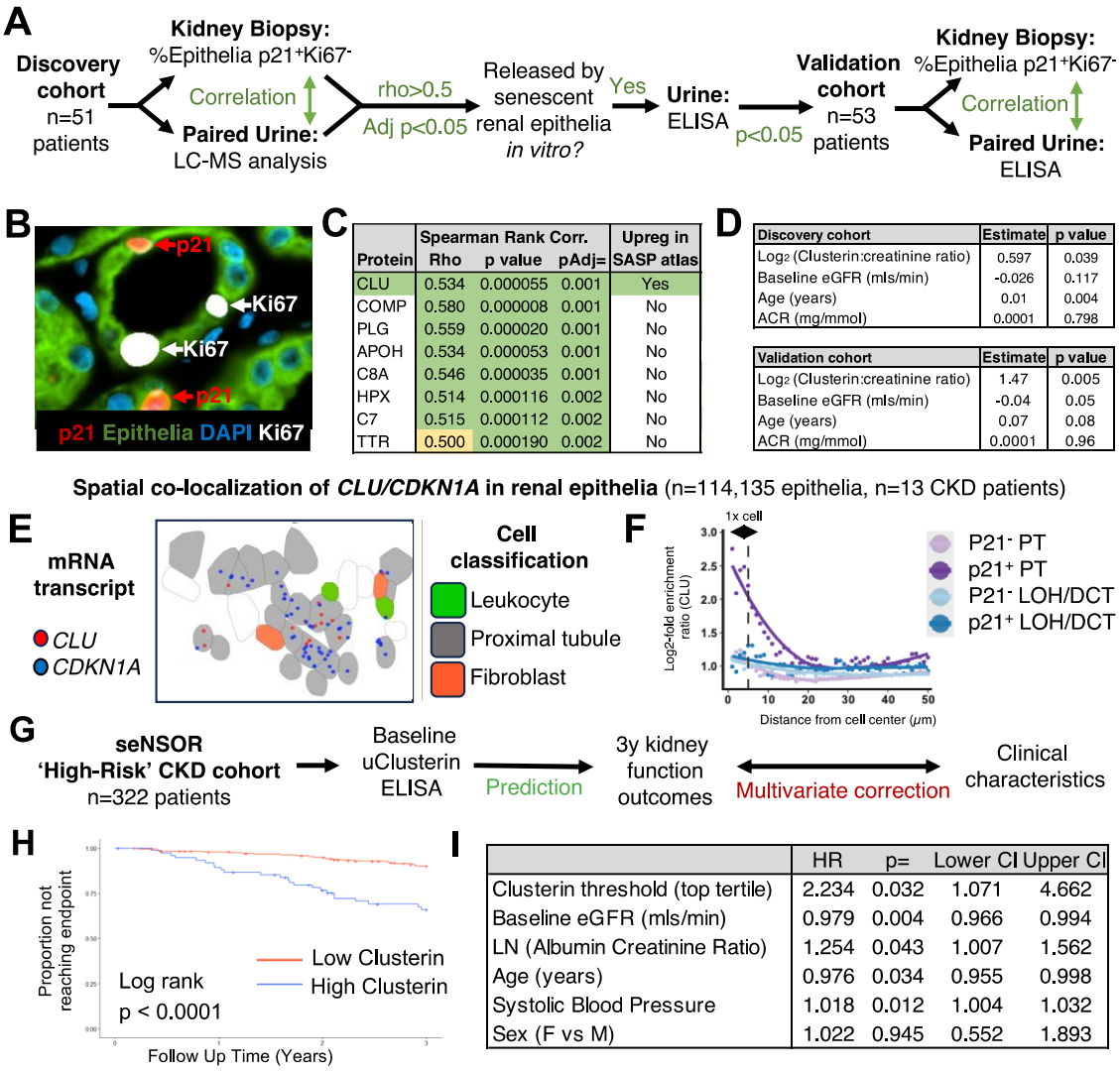

Figure Text: (**A**) Schema of cohort design for Discovery and Validation of urinary biomarkers of p21+Ki67- senescent epithelia. (**B**) Immunofluorescent staining of human renal biopsies. (**C**) Urinary proteins in LC-MS analysis correlating most closely with the proportion of p21+Ki67- senescent epithelial cells. (**D**) Discovery and Validation cohort linear regression analysis for predicting p21+Ki67- senescent epithelial cell proportions. (**E**) Image of CLU/CDKN1A co-localisation by spatial transcriptomic analysis. (**F**) Spatial enrichment (log2 scale) of CLU in proximity to $p21^{+}$ and $p21^{-}$ renal epithelial cells. (**G**) Schema of outcome studies in human CKD. (**H**) Proportion of patients with renal endpoint stratified by low (<124.5 μg/mmol) or high (>124.5 μg/mmol) Clusterin level. (**I**) Cox proportional hazards regression in outcome cohort.

Supplementary Materials and Methods

Sex as a biological variable

Our study examined male and female human patients with CKD, and findings are reported from both sexes.

seNSOR biobank recruitment

The seNSOR biobank comprised 635 patients recruited from renal clinics at the Royal Infirmary of Edinburgh, Edinburgh between March 2017 and March 2019. In addition, 100 patients with CKD were recruited to seNSOR from the Queen Elizabeth University Hospital, Glasgow between March 2018 and August 2019. Ethical approval was obtained from the Offices for Research Ethics Committee (REC/15/ES/0094, REC/20/ES/0061, REC 14/WS/1035 and REC 22/WS/0020) and informed patient consent and anonymisation undertaken in line with the Uniform Requirements of the International Committee of Medical Journal Editors as described previously. Participant information was collected upon enrollment with urine samples snap-frozen and stored at -80 °C.

In both centres, participant information collected upon enrolment included age, ethnicity, blood pressure and aetiology of CKD. Baseline and follow-up laboratory data obtained included serum creatinine. Glomerular filtration rate was estimated from serum creatinine using the 2009 Chronic Kidney Disease Epidemiology Collaboration (CKD-EPI) equation (1).

Patient selection for discovery and validation cohorts

The discovery cohort of 51 participants included all those recruited in Edinburgh with matched kidney tissue and urine samples available for analysis. The validation cohort included 53 participants that were recruited in Glasgow and also had matched kidney tissue and urine samples available. All kidney biopsies were performed for clinical indications by physicians independent of research team.

Patient selection for outcome analysis

Urine samples were available from 570 participants recruited into the seNSOR. 129 patients at low risk of CKD progression (baseline eGFR > 60 mls/min and ACR < 30mg/mmol) were excluded (Fig S1A). This matches the criterion used by other CKD biobanks (2). An additional 119 with baseline eGFR < 20 mls/min were excluded. The remaining 322 participants were included in the outcome analysis.

LC-MS analysis

LC-MS studies were undertaken on all urine samples in the discovery cohort by Lisa Imrie and Tessa Moses from the Edinomics Team (University of Edinburgh). Samples were depleted of high abundance proteins (serum albumin and IgG) using Agilent multiple affinity removal spin (MARS) cartridges following manufacturers protocol. They were trypsin digested using S-TrapTM (Protifi) following manufacturers protocol. After speed vac drying, peptide samples were re-suspended in MS-loading buffer (0.05% v/v trifluoroacetic acid in water) and 50 pmol of MassPREP Alcohol dehydrogenase (ADH) digestion standard (Waters) was spiked into each sample (added as an external standard). They were then filtered using Millex filter before HPLC-MS analysis.

Nano- Electrospray ionization (ESI)- High-performance liquid chromatography (HPLC)-MS/MS analysis was performed using an online system of a nano-HPLC (Dionex Ultimate 3000 RSLC, Thermo-Fisher Scientific) coupled to a QExactive mass spectrometer (Thermo-Fisher Scientific) with a 300 µm x 5 mm pre-column (Acclaim Pepmap, 5 µm particle size) joined with a 75 µm x 50 cm column (EASY- Spray, 3 µm particle size). The nano-pump was run using solvent A (2%Acetonitrile in water 0.1% formic acid) and solvent B (80% acetonitrile-20% water and 0.1% formic acid) and peptides were separated using a multi-step gradient of 2–98% buffer B at a flow rate of 300 nL/min over 90 min. Progenesis (version 4 Nonlinear Dynamics, UK) was used for LC-MS label-free quantitation. Filtering was carried out so that only MS/MS peaks with a charge of 2+, 3+ or 4+ were taken into account for the total number of ‘features’ (signal at one particular retention time and m/z) and only the five most intense spectra per ‘feature’ were included. MS/MS spectra was searched using MASCOT Version 2.4 (Matrix Science Ltd) against a UniProt *H.sapiens* database with maximum missed-cut

value set to 2. The following parameters were used in all searches: i) variable methionine oxidation, ii) fixed cysteine carbamidomethylation, iii) precursor mass tolerance of 10 ppm, iv) MS/MS tolerance of 0.05 Da, v) significance threshold (p) below 0.05 and vi) final peptide score of 20. Only proteins with 2 or more unique peptides were considered.

ELISA analysis

Urine Clusterin was measured on stored urine samples using R&D Duoset ELISAs (R&D Systems, Minneapolis, MN, catalogue number DY5874) with all samples run in duplicate. Based on pilot studies most samples were analysed following 1:1000 pre-dilution, with any results outside the published working range of the assay rerun at 1:100, 1 in 10,000 or 1:100,000 dilution.

Biochemical assays

Urinary creatinine measurements were determined using the creatininase/creatinase enzymatic method making use of a commercial kit (17654H, Sentinel Diagnostics via Alpha Laboratories Ltd., Eastleigh, UK) adapted for use on either a Cobas Fara or Mira analyser (Roche). Intra-assay precision was < 3% while inter-assay precision was CV < 5%. Urinary Clusterin was corrected for urinary creatinine throughout.

Microalbumin measurements were determined using a commercial kit (#1 0242 99 10 021, DiaSys Diagnostic Systems) adapted for use on a Cobas Mira analyser (Roche). This immunoturbidimetric assay was standardised against purified mouse albumin standards (Sigma Aldrich) with samples diluted in deionised water as appropriate. Intra-assay precision was < 5% while inter-assay precision was < 7.1%.

Tissue biopsy staining

Immunofluorescence staining on human kidney biopsy samples was performed using a BOND III automated immunostainer (Leica Biosystems) using sequential Tyramide-coupled fluorophores. Antibody concentrations were determined by titration of single immunofluorescent stains to determine the most suitable dilution before being combined into a multiplex stain. The immunofluorescent stain comprised 4 antibodies.

Pancytokeratin (CKPAN, Merck, Cat C2562) at 1:6000 dilution, and CD10 (Leica, Cat: NCL-L-CD10-270) at 1:600, both tubular epithelial markers, were added together, and the same Opal 520 fluorophore used for both. Other antibodies used in sequence targeted Ki67 (Agilent, Cat M724001-2) with an Opal 650 fluorophore and p21(Abcam, Cat ab109520) with an Opal 570 fluorophore (all secondary antibodies used at 1:500 dilution).

Microscopy and image analysis

Images of whole slides were acquired using the Axio Scan Z1 whole slide scanner (Zeiss, Jena, Germany). Images were then analysed using QUPath (version 0.3.2). Cells were classified automatically using the algorithm below based on nuclear staining of p21 and Ki67 as follows; p21 positive/Ki67 negative, Ki67 negative/p21 positive, double positive or double negative. Only tubular epithelia that were p21 positive and Ki67 negative were classed as having a cell cycle inhibitor profile consistent with senescence and this number was expressed as a percentage of all tubular cells. In participants where >1 section from their biopsy was available, the cell counts from each section were combined before percentages were calculated.

```
setImageType('FLUORESCENCE');
resetSelection(); createAnnotationsFromPixelClassifier("FindTissue", 0.0, 0.0)
selectAnnotations();
runPlugin('qupath.imagej.detect.cells.WatershedCellDetection', '{"detectionImage":
"DAPI", "requestedPixelSizeMicrons": 0.5, "backgroundRadiusMicrons": 8.0,
"medianRadiusMicrons": 0.0, "sigmaMicrons": 1.5, "minAreaMicrons": 10.0,
"maxAreaMicrons": 400.0, "threshold": 400.0, "watershedPostProcess": true,
"cellExpansionMicrons": 5.0, "includeNuclei": true, "smoothBoundaries": true,
"makeMeasurements": true}');
createAnnotationsFromPixelClassifier("FindTubules", 0.0, 0.0)
runObjectClassifier("DB_AI_6");
```

Spatial transcriptomic analysis

Spatial transcriptomic analysis was performed on kidney tissue from 13 patients; this included 9 core biopsies from patients in the discovery cohort (n=3 with minimal change disease and n = 6 with IgA nephropathy) and an additional 4 nephrectomy specimens from patients with fibrosis due to recurrent pyelonephritis (Table S1B). CDKN1A and CLU expression in sub-cellular resolution spatial transcriptomics data (NanoString CosMx SMI) was analysed using pre-processed data downloaded in Seurat (4.4.0) format from gene expression omnibus (GSE253439). The original cell annotations were used to classify proximal tubule (PT), or loop of Henle and distal convoluted tubule (LOH-DCT) cells which express CDKN1A (independent of cell state). To avoid false positive classifications due to noise in the assay and cell segmentation errors, cells were considered CDKN1A+ when at least 2 or more CDKN1A transcripts were detected within cell segmentation boundaries.

Spatial enrichment of CLU transcripts in relation to cell centroids of a given cell type were calculated as described previously (3). Briefly, for each individual cell, a search radius of 50μm in 1μm steps from the cell centroid was defined. For each given cell type, the number detected transcripts (of a given gene) were summed and normalised by the area of the circle segment and the number of cells encountered in the search area. Simultaneously, to calculate the background signal in the general cell population, 10,000 random cells were selected and the normalised transcript counts were calculated as before. The enrichment ratio at each interval was then defined as the log2+1-fold enrichment ratio of the query cell type over the randomly selected cell population. Cell boundaries and transcripts in 2D coordinates were visualised using the Seurat ImageDimPlot function.

Differential gene expression between CDKN1A+ and CDKN1A- PT cells was assessed using the Wilcoxon signed-rank test implemented by the Seurat function FindMarkers() with default parameters.

Statistical tests

Normality was assessed by Shapiro-Wilk test for all variables. Clinical characteristics for continuous data were expressed as mean ± standard deviation when data was

normally distributed and median (interquartile range) when not normally distributed. Categorical variables were expressed as counts. When comparing two unpaired groups, a T-test was used when the data was normally distributed, and a Mann-Whitney test used if the data was not normally distributed. Categorical values were assessed using a Chi-square test.

For the LC-MS data, values were corrected for ADH and then for urinary creatinine. To determine the linear correlation between each protein detected and histological p21+Ki67- epithelial cell proportions, correlation coefficients (rho) were estimated using Spearman's rank tests as the data was not normally distributed. Adjusted p values were calculated using the Benjamini and Hochberg False Discovery Rate (FDR) method from the list of p values, generated from the correlation between p21+Ki67- epithelial cell proportions and protein levels..

Linear regression was used to determine if levels of log2-tranformed Clusterin predicted histological p21+Ki67- epithelial cell proportions as the dependent variable in models alongside baseline eGFR, ACR and patient age.

Receiver operating characteristic (ROC) curve analysis was used to explore discrimination between those with top tertile Clusterin:Creatinine levels and determine the optimal cutoff point.

For the outcome analysis, CKD progression was defined as reaching ESKD (starting renal replacement therapy (RRT) or maintaining an eGFR <15mls/min for >90 days) or >40% reduction in renal function from eGFR at baseline (maintained for >90 days) (4) (5). Kaplan-Meier survival curves were constructed with the log-rank test used to compare curves. Univariate and multivariate analyses of outcomes using Cox proportional hazards survival models were performed. Death was treated as a censoring event. The proportional hazards assumption was tested and valid. A p value of less than 0.05 was considered significant.

All tests were performed using R version 4.1.2 or Graphpad Prism version 9.

Funding: DB is supported by MR/W00089X/1, DF is supported by MR/X006735/1. seNSOR is funded by RP_042_20160304 awarded to LD. LD is supported by SF_001_20181122

Supplementary References

1. Levey AS, et al. A new equation to estimate glomerular filtration rate. Ann Intern Med. 2009;150(9):604-12.
2. Taal MW, et al. Associations with age and glomerular filtration rate in a referred population with chronic kidney disease: methods and baseline data from a UK multicentre cohort study (NURTuRE-CKD). Nephrol Dial Transplant. 2023;38(11):2617-26.
3. Conway B, et al. Multiomic analysis of human kidney disease identifies a tractable inflammatory, pro-fibrotic tubular cell phenotype. 2024.
4. Levey AS, et al. GFR decline as an end point for clinical trials in CKD: a scientific workshop sponsored by the National Kidney Foundation and the US Food and Drug Administration. Am J Kidney Dis. 2014;64(6):821-35.
5. Levin A, et al. International consensus definitions of clinical trial outcomes for kidney failure: 2020. Kidney Int. 2020;98(4):849-59.

Supplementary Figure 1 Text: (**A**) Schema of patients included from the seNSOR biobank for the discovery, validation, and outcome analysis cohorts. (**B**) Immunofluorescent staining of human renal biopsies, same area as shown in Figure B but with selected channels as indicated and the QuPath annotations superimposed. (**C**) Correlation in the discovery cohort between the proportion of p21+Ki67- senescent epithelial cells and age. (**D**) Correlation in the discovery cohort between the proportion of p21+Ki67- senescent epithelial cells and ACR (**E**). Correlation in the discovery cohort between the proportion of p21+Ki67- senescent epithelial cells and estimated GFR. (**F**) Correlation between the proportion of p21+Ki67- senescent epithelial cells and urinary Clusterin:creatinine in the discovery cohort. (**G**) Correlation between the proportion of p21+Ki67- senescent epithelial cells and urinary Clusterin:creatinine in the validation cohort. (**H**) Receiver operating characteristic curve for urinary Clusterin:creatinine results discriminating between those in the highest tertile of p21+Ki67- senescent epithelial proportions and other participants.

Figure S1

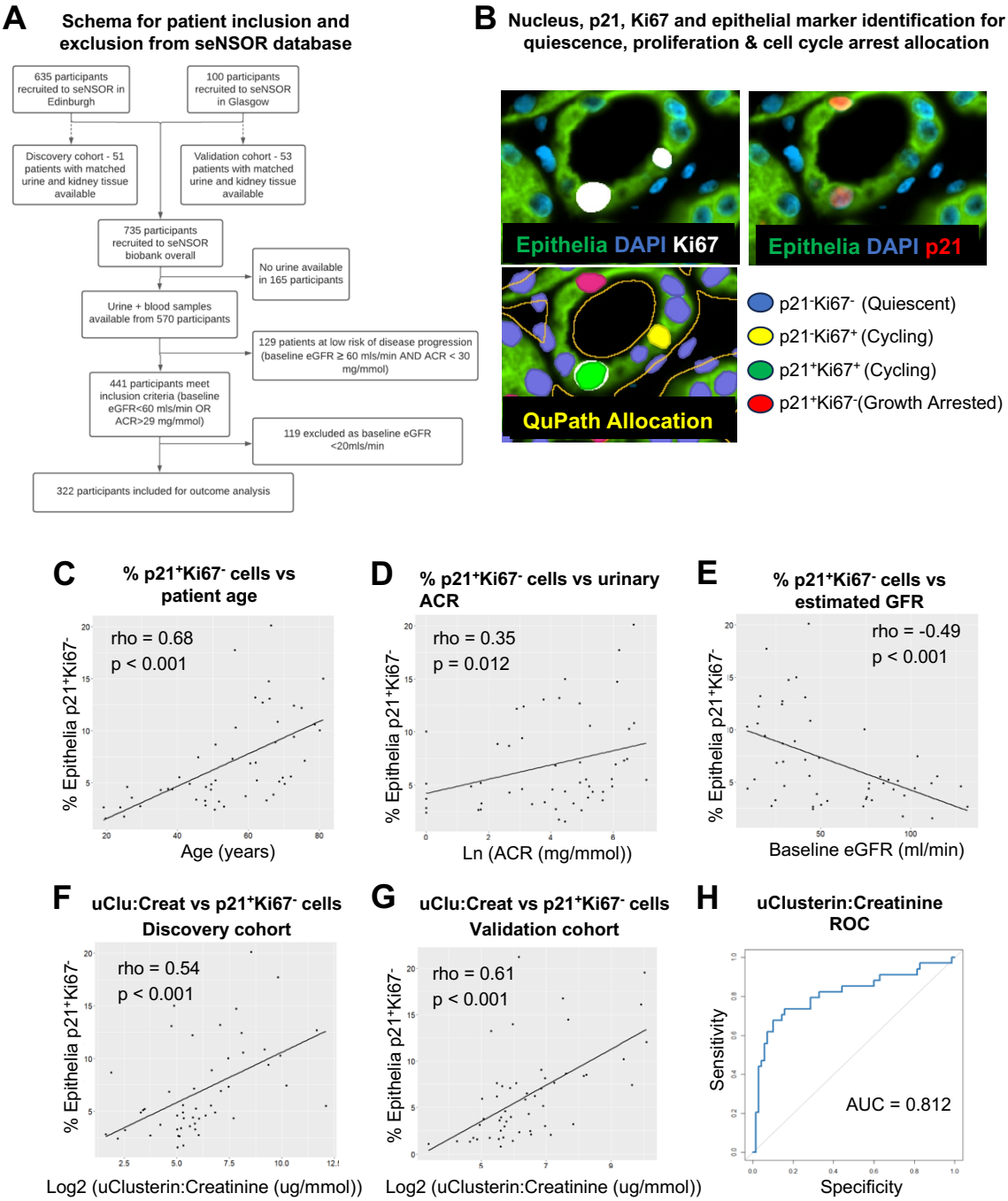
A
Schema for patient inclusion and exclusion from seNSOR database
635 participants recruited to seNSOR in Edinburgh
100 participants recruited to seNSOR in Glasgow
Discovery cohort - 51 patients with matched urine and kidney tissue available
Validation cohort - 53 patients with matched urine and kidney tissue available
735 participants recruited to seNSOR biobank overall
No urine available in 165 participants
Urine + blood samples available from 570 participants
129 patients at low risk of disease progression (baseline eGFR ≥ 60 mls/min AND ACR < 30 mg/mmol)
441 participants meet inclusion criteria (baseline eGFR<60 mls/min OR ACR>29 mg/mmol)
119 excluded as baseline eGFR <20mls/min
322 participants included for outcome analysis
B
Nucleus, p21, Ki67 and epithelial marker identification for quiescence, proliferation & cell cycle arrest allocation
Epithelia DAPI Ki67
Epithelia DAPI p21
QuPath Allocation
p21-Ki67- (Quiescent)
p21-Ki67+ (Cycling)
p21+Ki67+ (Cycling)
p21+Ki67-(Growth Arrested)
C
% p21+Ki67- cells vs patient age
rho = 0.68
p < 0.001
% Epithelia p21+Ki67-
Age (years)
D
% p21+Ki67- cells vs urinary ACR
rho = 0.35
p = 0.012
% Epithelia p21+Ki67-
Ln (ACR (mg/mmol))
E
% p21+Ki67- cells vs estimated GFR
rho = -0.49
p < 0.001
% Epithelia p21+Ki67-
Baseline eGFR (ml/min)
F
uClu:Creat vs p21+Ki67- cells
Discovery cohort
rho = 0.54
p < 0.001
% Epithelia p21+Ki67-
Log2 (uClusterin:Creatinine (ug/mmol))
G
uClu:Creat vs p21+Ki67- cells
Validation cohort
rho = 0.61
p < 0.001
% Epithelia p21+Ki67-
Log2 (uClusterin:Creatinine (ug/mmol))
H
uClusterin:Creatinine ROC
Sensitivity
AUC = 0.812
Specificity

Supplemental Table S1A. Baseline characteristics of discovery and validation cohorts.

	Discovery	Validation	p value for comparison
N	51	53	
Age (years), median (IQR)	56.2 (45.6, 67.4)	54.9 (37.1, 65.3)	0.61
Male/Female, n	32/19	29/24	0.53
eGFR (ml/min), median (IQR)	45.6 (28.8, 83.8)	47.1 (32.6, 84.2)	0.61
SBP, mean ± S.D	139 ± 21.8	139.5 ± 20.5	0.9
DBP, mean ± S.D	80.2 ± 12.4	82.5 ± 13.6	0.37
uACR (mg/mmol), median (IQR)	85.9 (16.4, 247.7)	131.2 (29.2, 333.2)	0.14
Ethnicity,			
White, n	47	43	
Black, n	1	0	
Asian, n	1	3	
Not recorded, n	2	7	
Diagnoses,			
IgA Nephropathy	21	9	
Membranous Nephropathy	0	7	
Interstitial Nephritis	6	8	
Minimal Change Disease	5	1	
Primary FSGS	0	4	
Diabetic Nephropathy	5	3	
Vasculitis	5	3	
Hypertensive / ischaemic nephropathy	2	5	
Lupus nephritis	2	3	
Other *	5	10	

* Other diagnoses in discovery cohort: Henoch-Schönlein purpura (n=2), lithium toxicity, obesity glomerulopathy and myeloma, and validation cohort: mesangiocapilllary glomerulonephritis (n=2), thin glomerular basement membrance (n=2), Henoch-Schönlein purpura, AA amyloid, AL amyloid, inflitration by lymphoma, CKD of uncertain aietiology and acute kidney injury.

Supplemental Table S1B. Baseline characteristics of outcome analysis cohorts

	Outcome cohort
N	322
Age (years), median (IQR).	60.5 (47.9, 69.3)
Male/Female, n	192/130
eGFR (ml/min/1.73m^2), median (IQR)	42.1 (29.8, 64.4)
SBP, median (IQR)	135 (122, 148)
DBP, median (IQR)	78 (70, 84)
uACR (mg/mmol), median (IQR)	81.6 (14.5, 288.8)
Ethnicity,	
White, n	279
Black, n	5
Asian, n	12
Not recorded, n	26
Diagnoses,	
Glomerular Disease	153
Tubulointerstitial Disease	44
Diabetes Mellitus	29
Renovascular disease / Hypertension	27
Other systemic diseases affecting kidney	7
Familial / Hereditary Nephropathies	10
Miscellaneous Renal Disorders	52

Supplemental Table S2. LC-MS protein correlations with proportion of p21+Ki67- senescent epithelia.

Gene	Protein	Rho	p value	Adjusted p value
COMP	Cartilage oligomeric matrix protein	0.580	0.00001	0.0033
PLG	Plasminogen	0.559	0.00002	0.0033
C8A	Complement component C8 alpha chain	0.546	0.00004	0.0040
APOH	Beta-2-glycoprotein 1	0.534	0.00005	0.0040
CLU	Clusterin	0.534	0.00006	0.0040
C7	Complement component C7	0.515	0.00011	0.0057
HPX	Hemopexin	0.514	0.00012	0.0057
TTR	Transthyretin	0.500	0.00019	0.0076
EFEMP1	EGF-containing fibulin-like extracellular matrix protein 1	0.494	0.00023	0.0076
PROS1	Vitamin K-dependent protein S	0.491	0.00025	0.0076
LUM	Lumican	0.489	0.00027	0.0076
FGA	Fibrinogen alpha chain	0.488	0.00028	0.0076
CTSD	Cathepsin D	0.486	0.00030	0.0076
SERPINA3	Alpha-1-antichymotrypsin	0.482	0.00035	0.0079
SERPING1	Plasma protease C1 inhibitor	0.480	0.00037	0.0079
C4A	Complement C4-A	0.479	0.00038	0.0079
C8G	Complement component C8 gamma chain	0.471	0.00049	0.0090
CFHR1	Complement factor H-related protein 1	0.471	0.00049	0.0090
SERPINC1	Antithrombin-III	0.464	0.00061	0.0099
IGLV3_21	NA	0.462	0.00063	0.0099
CRISP3	Cysteine-rich secretory protein 3 (Fragment)	0.462	0.00064	0.0099
F2	Prothrombin	0.461	0.00066	0.0099
GC_297	NA	0.457	0.00075	0.0107
GC_62	NA	0.455	0.00080	0.0107
C3	Complement C3	0.454	0.00081	0.0107
SERPINF1	Pigment epithelium-derived factor	0.451	0.00089	0.0113
GM2A	Ganglioside GM2 activator	0.445	0.00106	0.0128
ITIH4	ITIH4 protein	0.442	0.00115	0.0128
C9	Complement component C9	0.441	0.00119	0.0128
IGLC3	Ig lambda-3 chain C regions (Fragment)	0.440	0.00125	0.0128
HSPG2	Basement membrane-specific heparan sulfate proteoglycan core protein	0.439	0.00125	0.0128
C4BPA	C4b-binding protein alpha chain	0.438	0.00130	0.0128
AMBP	Protein AMBP	0.438	0.00130	0.0128
APOA1	Apolipoprotein A-I	0.437	0.00135	0.0128
PRG4	Proteoglycan 4	0.435	0.00142	0.0128
RNASE1	Ribonuclease pancreatic	0.435	0.00143	0.0128
IGLL5	Immunoglobulin lambda-like polypeptide 5	0.435	0.00143	0.0128
CFHR2	Complement factor H-related protein 2	0.432	0.00154	0.0132
PGLYRP2	N-acetylmuramoyl-L-alanine amidase	0.430	0.00165	0.0132
LDHB	L-lactate dehydrogenase B chain	0.430	0.00165	0.0132
RBP4	Retinol-binding protein 4	0.429	0.00170	0.0132

IGHA1	Ig alpha-1 chain C region	0.427	0.00180	0.0132
IGFBP6	Insulin-like growth factor-binding protein 6	0.427	0.00180	0.0132
WISP2	WNT1-inducible-signaling pathway protein 2	0.426	0.00183	0.0132
ORM1	Alpha-1-acid glycoprotein 1	0.426	0.00183	0.0132
ITIH2	Inter-alpha-trypsin inhibitor heavy chain H2	0.426	0.00184	0.0132
SLURP1	Secreted Ly-6/uPAR-related protein 1	0.421	0.00210	0.0148
C2	Complement C2	0.420	0.00214	0.0148
CFD	Complement factor D	0.416	0.00240	0.0162
APOD	Apolipoprotein D (Fragment)	0.413	0.00258	0.0171
FN1	Fibronectin	0.412	0.00267	0.0173
AGT	Angiotensinogen	0.409	0.00288	0.0183
IGHG1	Ig gamma-1 chain C region	0.407	0.00300	0.0187
LY6D	Lymphocyte antigen 6D	0.403	0.00333	0.0204
FBN1	Fibrillin-1	0.402	0.00348	0.0209
AHSG	Alpha-2-HS-glycoprotein	0.397	0.00388	0.0229
HRG	Histidine-rich glycoprotein	0.394	0.00424	0.0246
VTN	Vitronectin	0.392	0.00446	0.0251
UBA52	Ubiquitin-60S ribosomal protein L40 (Fragment)	0.392	0.00447	0.0251
IGFBP4	Insulin-like growth factor-binding protein 4	0.390	0.00469	0.0257
C8B	Complement component C8 beta chain	0.389	0.00481	0.0257
MSMB	Beta-microseminoprotein	0.389	0.00482	0.0257
IGLV2_11	NA	0.386	0.00512	0.0269
CP	Ceruloplasmin	0.382	0.00564	0.0289
CD5L	CD5 antigen-like	0.381	0.00576	0.0289
ITIH1	Inter-alpha-trypsin inhibitor heavy chain H1	0.381	0.00577	0.0289
NPC2	Epididymal secretory protein E1 (Fragment)	0.378	0.00619	0.0302
ORM2	Alpha-1-acid glycoprotein 2	0.378	0.00620	0.0302
GSN	Gelsolin	0.377	0.00634	0.0304
CPN2	Carboxypeptidase N subunit 2	0.375	0.00671	0.0317
PRSS2	Trypsin-2	0.374	0.00694	0.0324
CST6	Cystatin-M	0.372	0.00720	0.0331
SH3BGRL3	SH3 domain-binding glutamic acid-rich-like protein 3	0.371	0.00738	0.0335
FGB	Fibrinogen beta chain	0.365	0.00840	0.0375
TNFR1B	Soluble TNFR1B variant 1	0.365	0.00849	0.0375
PIGR	Polymeric immunoglobulin receptor	0.360	0.00939	0.0409
C5	Complement C5	0.359	0.00958	0.0412
VCAM1	Vascular cell adhesion protein 1	0.356	0.01035	0.0439
FETUB	Fetuin-B	0.354	0.01092	0.0458
NBL1	Neuroblastoma suppressor of tumorigenicity 1	0.350	0.01185	0.0490
CFH	Complement factor H	0.349	0.01208	0.0494
CD59	CD59 glycoprotein	0.347	0.01264	0.0506
ENO1	Alpha-enolase	0.346	0.01279	0.0506
PFN1	Profilin-1	0.346	0.01284	0.0506
LY6H	Lymphocyte antigen 6H	0.344	0.01345	0.0522
IGLC7	Ig lambda-7 chain C region	0.344	0.01356	0.0522
SERPINF2	Alpha-2-antiplasmin	0.343	0.01388	0.0526

KNG1	Kininogen-1	0.342	0.01398	0.0526
IGHG4	Ig gamma-4 chain C region (Fragment)	0.341	0.01426	0.0530
AMY2A	Pancreatic alpha-amylase	0.339	0.01501	0.0549
YWHAB	14-3-3 protein beta/alpha	0.339	0.01510	0.0549
IGHV3_72	NA	0.338	0.01527	0.0549
MT2A	Metallothionein-2	0.337	0.01550	0.0552
CD14	Monocyte differentiation antigen CD14	0.336	0.01607	0.0562
CST3	Cystatin-C	0.335	0.01623	0.0562
CA1	Carbonic anhydrase 1	0.335	0.01629	0.0562
APOA4	Apolipoprotein A-IV	0.334	0.01666	0.0569
IGHA2	Ig alpha-2 chain C region (Fragment)	0.332	0.01739	0.0587
APOA2	Apolipoprotein A-II (Fragment)	0.331	0.01779	0.0595
PTGDS	Prostaglandin-H2 D-isomerase	0.330	0.01819	0.0602
THY1	Thy-1 membrane glycoprotein	0.328	0.01863	0.0611
C1RL	Complement C1r subcomponent-like protein	0.328	0.01884	0.0611
EFNA1	Ephrin-A1	0.326	0.01958	0.0623
AZGP1	Zinc-alpha-2-glycoprotein	0.326	0.01958	0.0623
SOD1	Superoxide dismutase [Cu-Zn]	0.325	0.02012	0.0634
ENDOD1	Endonuclease domain-containing 1 protein	0.323	0.02064	0.0640
ECM1	Extracellular matrix protein 1	0.323	0.02068	0.0640
IGKV2D_28	NA	0.323	0.02087	0.0640
VSIG4	V-set and immunoglobulin domain-containing protein 4	0.318	0.02288	0.0695
F12	Coagulation factor XII	0.314	0.02465	0.0742
FBLN1	Fibulin-1	0.314	0.02496	0.0744
AGRN	Agrin	0.312	0.02572	0.0760
IGFBP1	Insulin-like growth factor-binding protein 1	0.310	0.02701	0.0791
HP	Haptoglobin	0.309	0.02758	0.0801
LRG1	Leucine-rich alpha-2-glycoprotein	0.308	0.02811	0.0809
ELANE	Neutrophil elastase	0.307	0.02860	0.0816
CHIT1	Chitotriosidase-1	0.306	0.02919	0.0823
JCHAIN	Immunoglobulin J chain (Fragment)	0.305	0.02935	0.0823
APOE	Apolipoprotein E	0.305	0.02972	0.0827
YWHAZ	14-3-3 protein zeta/delta (Fragment)	0.302	0.03134	0.0865
PEBP4	Phosphatidylethanolamine-binding protein 4	0.300	0.03267	0.0894
C6	Complement component C6	0.290	0.03877	0.1052
PROZ	Vitamin K-dependent protein Z	0.286	0.04188	0.1123
TF	Serotransferrin	0.286	0.04226	0.1123
CDH1	Cadherin-1	0.285	0.04267	0.1123
IGFBP7	Insulin-like growth factor-binding protein 7	0.285	0.04274	0.1123
CTSB	Cathepsin B	0.283	0.04420	0.1152
APOL1	Apolipoprotein L1	0.283	0.04456	0.1152
ESAM	Endothelial cell-selective adhesion molecule	0.281	0.04556	0.1169
FABP4	Fatty acid-binding protein, adipocyte	0.279	0.04733	0.1205
LGALS3BP	Galectin-3-binding protein	0.273	0.05289	0.1336
IGFBP3	Insulin-like growth factor-binding protein 3 (Fragment)	0.272	0.05348	0.1341
KRT81	Keratin, type II cuticular Hb1	-0.271	0.05407	0.1346

A1BG	Alpha-1B-glycoprotein	0.270	0.05539	0.1368
COL18A1	Collagen alpha-1(XVIII) chain (Fragment)	0.269	0.05607	0.1375
FGG	Fibrinogen gamma chain	0.266	0.05896	0.1430
MMP9	Matrix metalloproteinase-9	0.266	0.05918	0.1430
A2M	Alpha-2-macroglobulin	0.264	0.06077	0.1458
ARSA	Arylsulfatase A	0.263	0.06206	0.1478
MST1L	Putative macrophage stimulating 1-like protein	0.263	0.06251	0.1478
MYH9	Myosin-9	0.262	0.06326	0.1485
LCN2	Neutrophil gelatinase-associated lipocalin	0.261	0.06472	0.1509
DEFB1	Beta-defensin 1	0.260	0.06563	0.1519
AFM	Afamin	0.255	0.07060	0.1623
CORO1A	Coronin-1A	0.254	0.07165	0.1636
SIRPA	Tyrosine-protein phosphatase non-receptor type substrate 1	0.253	0.07279	0.1650
LYZ	Lysozyme C	0.251	0.07526	0.1695
MPO	Myeloperoxidase	0.251	0.07591	0.1698
LTF	Lactotransferrin	0.250	0.07701	0.1711
ALDOA	Fructose-bisphosphate aldolase	0.249	0.07851	0.1733
CD248	Endosialin	0.248	0.07924	0.1737
LTBP2	Latent-transforming growth factor beta-binding protein 2	0.246	0.08130	0.1770
SPP1	Osteopontin	0.242	0.08748	0.1893
TFF2	Trefoil factor 2	-0.240	0.08932	0.1920
ENPEP	Glutamyl aminopeptidase	0.238	0.09321	0.1991
SIRPB1	Signal-regulatory protein beta-1	0.236	0.09530	0.2022
PRDX2	Peroxiredoxin-2	0.235	0.09672	0.2039
IGKV6_21	NA	0.233	0.09922	0.2079
PGLYRP1	Peptidoglycan recognition protein 1	0.231	0.10285	0.2141
RNASET2	Ribonuclease T2	0.230	0.10467	0.2160
HLA_B	NA	0.230	0.10505	0.2160
KLK6	Kallikrein-6	0.229	0.10678	0.2182
CALR	Calreticulin	0.228	0.10807	0.2195
HABP2	Hyaluronan-binding protein 2	0.226	0.11054	0.2231
COTL1	Coactosin-like protein	0.226	0.11139	0.2235
PON1	Serum paraoxonase/arylesterase 1	0.224	0.11335	0.2260
DSC1	Desmocollin-1	0.223	0.11493	0.2278
ACTB	Actin, cytoplasmic 1	0.223	0.11652	0.2296
ITIH3	Inter-alpha-trypsin inhibitor heavy chain H3	0.219	0.12337	0.2416
IGFBP5	Insulin-like growth factor-binding protein 5 (Fragment)	0.217	0.12660	0.2465
KLKB1	Plasma kallikrein (Fragment)	0.215	0.12927	0.2502
RNASE2	Non-secretory ribonuclease	0.214	0.13170	0.2523
LYVE1	Lymphatic vessel endothelial hyaluronic acid receptor 1	0.214	0.13185	0.2523
VMO1	Vitelline membrane outer layer protein 1 homolog	0.213	0.13290	0.2528
LYNX1_192	NA	0.211	0.13747	0.2600
PI16	Peptidase inhibitor 16	0.210	0.13991	0.2631
HSPA1A	Heat shock 70 kDa protein 1A	0.208	0.14303	0.2675
RNASE4	Ribonuclease 4	0.207	0.14559	0.2702
SECTM1	Secreted and transmembrane protein 1 (Fragment)	0.206	0.14613	0.2702

EFNB1	Ephrin-B1	0.206	0.14777	0.2717
LMAN2	Vesicular integral-membrane protein VIP36	0.199	0.16249	0.2972
CD44	CD44 antigen (Fragment)	0.198	0.16406	0.2984
FAM3C	Protein FAM3C	0.193	0.17556	0.3175
SERPINA5	Plasma serine protease inhibitor	0.191	0.17972	0.3233
CFI	Complement factor I	0.185	0.19488	0.3487
F13B	Coagulation factor XIII B chain	0.184	0.19666	0.3500
B2M	Beta-2-microglobulin	0.183	0.19847	0.3513
MGAM	Maltase-glucoamylase, intestinal (Fragment)	0.181	0.20252	0.3558
LPA	Apolipoprotein(a)	0.181	0.20348	0.3558
RETN	Resistin	0.180	0.20499	0.3558
CHGA	Chromogranin-A	-0.180	0.20531	0.3558
MFAP5	Microfibrillar-associated protein 5 (Fragment)	0.178	0.21237	0.3644
PVRL2	Nectin-2	0.177	0.21304	0.3644
C1QB	Complement C1q subcomponent subunit B (Fragment)	0.177	0.21434	0.3644
LTBP1	Latent-transforming growth factor beta-binding protein 1	0.176	0.21639	0.3644
SERPIND1	Heparin cofactor 2	0.176	0.21674	0.3644
REG1A	Lithostathine-1-alpha	0.176	0.21687	0.3644
C1S	Complement C1s subcomponent	0.175	0.21815	0.3647
GKN1	Gastrokine-1	0.174	0.22147	0.3684
CD40	CD40 antigen (TNF receptor superfamily member 5), isoform CRA_c	0.173	0.22406	0.3708
ANPEP	Aminopeptidase N	0.173	0.22515	0.3708
HIST1H2AG	Histone H2A type 1	0.169	0.23694	0.3883
COL15A1	Collagen alpha-1(XV) chain	0.165	0.24744	0.4035
PSAP	Prosaposin	0.164	0.25096	0.4053
PAPPA2	Pappalysin-2	0.163	0.25193	0.4053
ICAM1	Intercellular adhesion molecule 1	0.163	0.25226	0.4053
ROBO4	Roundabout homolog 4	0.163	0.25390	0.4060
ATRN	Attractin	0.162	0.25609	0.4069
F10	Coagulation factor X	0.162	0.25692	0.4069
FABP1	Fatty acid-binding protein, liver	0.159	0.26646	0.4200
SCUBE2	Signal peptide, CUB and EGF-like domain-containing protein 2	0.158	0.26922	0.4223
C1R	Complement C1r subcomponent	-0.157	0.27229	0.4251
IGLV2_14	NA	0.153	0.28334	0.4403
BTN2A1	Butyrophilin subfamily 2 member A1	-0.152	0.28743	0.4446
MEP1A	Metalloendopeptidase	0.150	0.29270	0.4506
SPINK5	Serine protease inhibitor Kazal-type 5	0.148	0.30070	0.4601
MASP2	Mannan-binding lectin serine protease 2	0.148	0.30161	0.4601
SCGB1A1	Uteroglobin	0.146	0.30643	0.4636
CFP	Properdin	0.146	0.30738	0.4636
SERPINA4	Kallistatin	-0.146	0.30811	0.4636
HGFAC	Hepatocyte growth factor activator	0.143	0.31776	0.4759
MB	Myoglobin (Fragment)	0.141	0.32212	0.4803
ART3	NAD(P)(+)--arginine ADP-ribosyltransferase (Fragment)	0.140	0.32889	0.4882
ANXA2	Annexin (Fragment)	0.137	0.33607	0.4966

F9	Coagulation factor IX	0.136	0.34027	0.4991
FLNA	Filamin-A	0.136	0.34080	0.4991
CDH6	Cadherin-6	-0.132	0.35410	0.5163
PRNP	Major prion protein (Fragment)	0.130	0.36194	0.5255
DSC3	Desmocollin-3	-0.129	0.36802	0.5319
SERPINA7	Thyroxine-binding globulin	0.126	0.37737	0.5431
TWSG1	Twisted gastrulation protein homolog 1	0.124	0.38780	0.5557
CAPG	Macrophage-capping protein (Fragment)	-0.121	0.39675	0.5641
COL6A1	Collagen alpha-1(VI) chain	0.121	0.39804	0.5641
PSCA	Prostate stem cell antigen	0.121	0.39882	0.5641
PPBP	Platelet basic protein	0.120	0.40299	0.5676
CDH13	Cadherin-13	0.119	0.40519	0.5683
HYOU1	Hypoxia up-regulated protein 1	0.118	0.40914	0.5714
CTGF	Connective tissue growth factor	0.117	0.41205	0.5725
TXNDC5	Thioredoxin domain-containing protein 5	0.117	0.41371	0.5725
TXN	Thioredoxin	0.117	0.41511	0.5725
GNS	N-acetylglucosamine-6-sulfatase	0.115	0.42045	0.5775
CAMP	Cathelicidin antimicrobial peptide	0.114	0.42709	0.5814
HIST1H1E	Histone H1.4	0.113	0.42849	0.5814
DKK3	Dickkopf-related protein 3	0.113	0.42857	0.5814
SPARCL1	SPARC-like protein 1	0.110	0.44250	0.5973
PRSS1	Protease serine 1	-0.110	0.44394	0.5973
TNFRSF1A	Tumor necrosis factor receptor superfamily member 1A (Fragment)	0.109	0.44715	0.5992
WFDC2	WAP four-disulfide core domain protein 2	0.108	0.44926	0.5996
ANXA1	Annexin A1	0.107	0.45538	0.6046
CD27	CD27 antigen	0.106	0.45845	0.6046
CCL14	C-C motif chemokine 14	0.106	0.45845	0.6046
PEBP1	Phosphatidylethanolamine-binding protein 1	-0.104	0.46697	0.6124
IGFBP2	Insulin-like growth factor-binding protein 2	0.104	0.46810	0.6124
KRT9	Keratin, type I cytoskeletal 9	0.102	0.47676	0.6193
LRP2	Low-density lipoprotein receptor-related protein 2	0.102	0.47711	0.6193
HBB	Hemoglobin subunit beta	0.101	0.47912	0.6195
ASAH1	Acid ceramidase	0.096	0.50248	0.6446
SERPINB1	Leukocyte elastase inhibitor	-0.095	0.50534	0.6446
PCOLCE	Procollagen C-endopeptidase enhancer 1	0.095	0.50633	0.6446
APOB	Apolipoprotein B-100	0.095	0.50634	0.6446
COL5A1	Collagen alpha-1(V) chain	0.094	0.51127	0.6475
CD300A	CMRF35-like molecule 8	0.094	0.51255	0.6475
SEMG1	Semenogelin-1	0.091	0.52673	0.6626
PGA4	Pepsin A-4	0.090	0.52851	0.6626
TPI1	Triosephosphate isomerase	0.089	0.53391	0.6669
IGHG3	Ig gamma-3 chain C region	0.089	0.53642	0.6675
MCAM	Cell surface glycoprotein MUC18	0.088	0.53890	0.6681
LAMP1	Lysosome-associated membrane glycoprotein 1	0.086	0.54860	0.6776
CD300LG	CMRF35-like molecule 9	0.081	0.57250	0.7045

LOX	Protein-lysine 6-oxidase	0.079	0.58115	0.7125
AHCY	Adenosylhomocysteinase	0.076	0.59598	0.7279
CDH11	Cadherin-11	-0.075	0.60242	0.7331
FLG	Filaggrin	-0.072	0.61342	0.7428
PILRA	Paired immunoglobulin-like type 2 receptor alpha (Fragment)	0.072	0.61491	0.7428
FCGR3B	Low affinity immunoglobulin gamma Fc region receptor III-B	0.071	0.61889	0.7449
HIST1H4A	Histone H4	0.071	0.62168	0.7456
SH3BGRL	SH3 domain-binding glutamic acid-rich-like protein	0.069	0.62809	0.7505
RNASE6	Ribonuclease K6	0.068	0.63469	0.7557
SERPINB3	SCCA1/SCCA2 fusion protein	-0.065	0.64963	0.7679
FSTL1	Follistatin-related protein 1 (Fragment)	0.064	0.65377	0.7679
TKT	Transketolase	-0.064	0.65393	0.7679
NID1	Nidogen-1	-0.064	0.65419	0.7679
CD55	Complement decay-accelerating factor	0.062	0.66380	0.7764
LCP1	Plastin-2	-0.058	0.68740	0.7951
VWF	von Willebrand factor	0.058	0.68765	0.7951
HMCN1	Hemicentin-1 (Fragment)	0.058	0.68838	0.7951
CADM3	Cell adhesion molecule 3 (Fragment)	0.057	0.68939	0.7951
KRT16	Keratin, type I cytoskeletal 16	-0.054	0.70464	0.8081
IGF2	Insulin-like growth factor II	0.054	0.70557	0.8081
COL6A3	Collagen alpha-3(VI) chain	0.053	0.71445	0.8130
CRNN	Cornulin	0.052	0.71474	0.8130
EGF	Pro-epidermal growth factor	-0.051	0.71968	0.8131
PVR	Poliovirus receptor	0.051	0.71973	0.8131
CHI3L1	Chitinase-3-like protein 1	-0.050	0.72989	0.8218
KRT5	Keratin, type II cytoskeletal 5	-0.048	0.73821	0.8283
HBA1	Hemoglobin subunit alpha	0.046	0.74919	0.8364
SERPINA6	Corticosteroid-binding globulin	0.045	0.75254	0.8364
S100A9	Protein S100-A9	0.045	0.75301	0.8364
EPHA1	Ephrin type-A receptor 1	0.044	0.76057	0.8420
HIST1H2BE	Histone H2B	0.043	0.76541	0.8423
KRT2	Keratin, type II cytoskeletal 2 epidermal	0.043	0.76599	0.8423
FOLR1	Folate receptor alpha	-0.042	0.77123	0.8453
UMOD	Uromodulin	-0.041	0.77420	0.8457
KRT1	Keratin, type II cytoskeletal 1	0.040	0.77855	0.8477
KLK3	Prostate-specific antigen (Fragment)	0.038	0.79063	0.8580
FLNC	Filamin-C	0.037	0.79675	0.8618
CTSZ	Cathepsin Z	0.036	0.80138	0.8640
KRT14	Keratin, type I cytoskeletal 14	-0.030	0.83274	0.8931
DAG1	Dystroglycan	-0.030	0.83377	0.8931
CEACAM8	Carcinoembryonic antigen-related cell adhesion molecule 8	0.029	0.83840	0.8952
KPRP	Keratinocyte proline-rich protein	0.028	0.84704	0.9015
MSN	Moesin	0.026	0.85879	0.9111
SOD3	Extracellular superoxide dismutase [Cu-Zn]	-0.022	0.87566	0.9239
CRHBP	Corticotropin-releasing factor-binding protein	0.022	0.87749	0.9239
KRT10	Keratin, type I cytoskeletal 10	-0.022	0.87926	0.9239

ALB	Serum albumin	0.021	0.88374	0.9249
KRT6A	Keratin, type II cytoskeletal 6A	-0.021	0.88573	0.9249
LBP	Lipopolysaccharide-binding protein	0.019	0.89469	0.9301
NEGR1	Neuronal growth regulator 1	0.018	0.89761	0.9301
KLK1	Kallikrein-1	-0.018	0.89918	0.9301
FLG2	Filaggrin-2	0.017	0.90355	0.9317
HRNR	Hornerin	-0.015	0.91517	0.9408
TPM3	Tropomyosin alpha-3 chain	0.014	0.92015	0.9429
TALDO1	Transaldolase	0.013	0.92676	0.9460
FABP5	Fatty acid-binding protein, epidermal	-0.012	0.93069	0.9460
LYNX1_264	NA	0.012	0.93169	0.9460
FOLR2	Folate receptor beta	-0.010	0.94397	0.9555
SUMF2	Sulfatase-modifying factor 2	-0.008	0.95471	0.9626
GRN	Granulins	-0.008	0.95677	0.9626
IFI30	Gamma-interferon-inducible lysosomal thiol reductase	0.006	0.96481	0.9677
FCGBP	IgGFc-binding protein	0.004	0.97838	0.9784

Supplemental Table S3A. Cox Proportional Hazards models.

Clusterin - using threshold				
	Hazard ratio	p	Lower CI	Upper CI
Clusterin threhsold (above vs below)	2.234	0.032	1.071	4.662
Baseline eGFR (mls/min)	0.979	0.004	0.966	0.994
LN (Albumin Creatinine Ratio)	1.254	0.043	1.007	1.562
Age (years)	0.976	0.034	0.955	0.998
Systolic Blood Pressure	1.018	0.012	1.004	1.032
Sex (F vs M)	1.022	0.945	0.552	1.893

Clusterin - using continuous values				
	Hazard ratio	p	Lower CI	Upper CI
Clusterin:Creatinine ratio per 100 µg/mmol	1.060	0.002	1.022	1.099
Baseline eGFR (mls/min)	0.977	0.002	0.964	0.991
LN (Albumin Creatinine Ratio)	1.321	0.005	1.090	1.602
Age (years)	0.974	0.021	0.952	0.996
Systolic Blood Pressure	1.020	0.005	1.006	1.033
Sex (F vs M)	1.102	0.759	0.593	2.049

Clusterin - using log tranformed values				
	Hazard ratio	p	Lower CI	Upper CI
Log2 (Clusterin:Creatinine)	1.33	0.01	1.07	1.64
Baseline eGFR (mls/min)	0.98	0.01	0.97	0.99
LN (Albumin Creatinine Ratio)	1.15	0.24	0.91	1.46
Age (years)	0.98	0.02	0.95	1.00
Systolic Blood Pressure	1.02	0.01	1.00	1.03
Sex (F vs M)	1.07	0.84	0.57	1.99